NASA/TM—2010-216895

AIAA–2010–6701

Thrust Stand Characterization of the NASA Evolutionary Xenon Thruster (NEXT)

Kevin D. Diamant, James E. Pollard, and Mark W. Crofton
The Aerospace Corporation, El Segundo, California

Michael J. Patterson and George C. Soulas
Glenn Research Center, Cleveland, Ohio

November 2010

NASA STI Program . . . in Profile

Since its founding, NASA has been dedicated to the advancement of aeronautics and space science. The NASA Scientific and Technical Information (STI) program plays a key part in helping NASA maintain this important role.

The NASA STI Program operates under the auspices of the Agency Chief Information Officer. It collects, organizes, provides for archiving, and disseminates NASA's STI. The NASA STI program provides access to the NASA Aeronautics and Space Database and its public interface, the NASA Technical Reports Server, thus providing one of the largest collections of aeronautical and space science STI in the world. Results are published in both non-NASA channels and by NASA in the NASA STI Report Series, which includes the following report types:

- TECHNICAL PUBLICATION. Reports of completed research or a major significant phase of research that present the results of NASA programs and include extensive data or theoretical analysis. Includes compilations of significant scientific and technical data and information deemed to be of continuing reference value. NASA counterpart of peer-reviewed formal professional papers but has less stringent limitations on manuscript length and extent of graphic presentations.

- TECHNICAL MEMORANDUM. Scientific and technical findings that are preliminary or of specialized interest, e.g., quick release reports, working papers, and bibliographies that contain minimal annotation. Does not contain extensive analysis.

- CONTRACTOR REPORT. Scientific and technical findings by NASA-sponsored contractors and grantees.

- CONFERENCE PUBLICATION. Collected papers from scientific and technical conferences, symposia, seminars, or other meetings sponsored or cosponsored by NASA.

- SPECIAL PUBLICATION. Scientific, technical, or historical information from NASA programs, projects, and missions, often concerned with subjects having substantial public interest.

- TECHNICAL TRANSLATION. English-language translations of foreign scientific and technical material pertinent to NASA's mission.

Specialized services also include creating custom thesauri, building customized databases, organizing and publishing research results.

For more information about the NASA STI program, see the following:

- Access the NASA STI program home page at *http://www.sti.nasa.gov*

- E-mail your question via the Internet to *help@sti.nasa.gov*

- Fax your question to the NASA STI Help Desk at 443–757–5803

- Telephone the NASA STI Help Desk at 443–757–5802

- Write to:
  NASA Center for AeroSpace Information (CASI)
  7115 Standard Drive
  Hanover, MD 21076–1320

NASA/TM—2010-216895

AIAA–2010–6701

Thrust Stand Characterization of the NASA Evolutionary Xenon Thruster (NEXT)

Kevin D. Diamant, James E. Pollard, and Mark W. Crofton
The Aerospace Corporation, El Segundo, California

Michael J. Patterson and George C. Soulas
Glenn Research Center, Cleveland, Ohio

Prepared for the
46th Joint Propulsion Conference and Exhibit
cosponsored by the AIAA, ASME, SAE, and ASEE
Nashville, Tennessee, July 25–28, 2010

National Aeronautics and
Space Administration

Glenn Research Center
Cleveland, Ohio 44135

November 2010

Acknowledgments

The authors thank Kevin McCormick of the NASA Glenn Research Center for outstanding technical support throughout the process of thruster installation, and Mike Worshum, Tom Albright, and Dave Rikimaru of The Aerospace Corporation for many excellent suggestions and outstanding technical support in the development and construction of the thrust stand. Robert Csortos of Dura Magnetics, Inc., designed the eddy current damper magnet assembly. Special thanks to George Valenzuela of The Aerospace Corporation for explaining some of the finer points of fishing line usage, and to Dan Herman of the NASA Glenn Research Center for many helpful suggestions. This work was supported under The Aerospace Corporation's Independent Research and Development Program.

This report contains preliminary findings, subject to revision as analysis proceeds.

Level of Review: This material has been technically reviewed by technical management.

Available from

NASA Center for Aerospace Information
7115 Standard Drive
Hanover, MD 21076–1320

National Technical Information Service
5301 Shawnee Road
Alexandria, VA 22312

Available electronically at http://gltrs.grc.nasa.gov

Thrust Stand Characterization of the NASA Evolutionary Xenon Thruster (NEXT)

Kevin D. Diamant, James E. Pollard, and Mark W. Crofton
The Aerospace Corporation
El Segundo, California 90245

Michael J. Patterson and George C. Soulas
National Aeronautics and Space Administration
Glenn Research Center
Cleveland, Ohio 44135

Abstract

Direct thrust measurements have been made on the NASA Evolutionary Xenon Thruster (NEXT) ion engine using a standard pendulum style thrust stand constructed specifically for this application. Values have been obtained for the full 40-level throttle table, as well as for a few off-nominal operating conditions. Measurements differ from the nominal NASA throttle table 10 (TT10) values by 3.1 percent at most, while at 30 throttle levels (TLs) the difference is less than 2.0 percent. When measurements are compared to TT10 values that have been corrected using ion beam current density and charge state data obtained at The Aerospace Corporation, they differ by 1.2 percent at most, and by 1.0 percent or less at 37 TLs. Thrust correction factors calculated from direct thrust measurements and from The Aerospace Corporation's plume data agree to within measurement error for all but one TL. Thrust due to cold flow and "discharge only" operation has been measured, and analytical expressions are presented which accurately predict thrust based on thermal thrust generation mechanisms.

1.0 Introduction

NASA's Evolutionary Xenon Thruster (NEXT) is engineered to be extremely flexible in terms of input power and specific impulse, while maintaining acceptable efficiency, and embodies a number of advances over previous ion engine systems. Some of its operating characteristics are being examined in detail in a study conducted in a test facility at The Aerospace Corporation (Ref. 1). The work is performed under the umbrella of a Space Act Agreement, with NASA participation in readying and operating the hardware under test.

The NEXT throttle table was developed for missions outside of Earth orbit, and incorporates 40 levels to account for varying solar power with sun-spacecraft separation. Prior to this work, thrust has been estimated from terminal parameters and available plume data. Recent plume measurements at The Aerospace Corporation have improved the fidelity of those estimates(Ref. 2), however direct thrust measurements are needed for benchmarking.

The majority of thrust measurements reported in the electric propulsion literature have been made indirectly, by measuring deflection of the mechanism to which the thruster is mounted, and converting that deflection to thrust through some suitable calibration. The mechanism is generally a pendulum, either standard (Refs. 3 to 7), inverted (Refs. 8 to 10), or torsional (Refs. 11 to 14), and calibration is accomplished through application of a set of weights. By contrast, high thrust chemical engines are generally tested with load cells (e.g. Ref. 15). The availability of load cells with sufficient sensitivity permitted their introduction by Crofton (Ref. 16) and Brady (Ref. 17) to low thrust measurement applications. Advantages conferred through the use of load cells are high accuracy over a wide measurement range due to their high degree of linearity, the limiting of thrust stand motion to very small values, and prompt readings. With regard to the latter, there is no need for time-consuming force-displacement calibrations, during which thermal drift may introduce uncertainty into the measurement. The use of load cells for low thrust measurements has been

demonstrated in References 18 to 20, and is the method adopted here to measure thrust due to ion beam extraction. However, the sensitivity required to accurately measure thrust during operation without ion beam extraction (cold flow and "discharge only") exceeded the capability of the load cell, and those measurements were made using an inclinometer along with a set of calibration weights.

2.0 Test Apparatus

Measurements were performed in a 2.4-m diameter by 9.8-m long cryopumped vacuum chamber with the thruster oriented along the chamber centerline. Two re-entrant pumps were on the end-dome behind the thruster, two more re-entrant pumps were in the beam dump region, and four 1.3-m cryotubs were mounted on the cylindrical wall of the tank adjacent to the thruster. The base pressure with no gas load was less than 1×10^{-7} torr, with 90 percent of the residual gas being water vapor, and the remainder being air and hydrocarbons. The beam dump was lined with carbon composite sheets and flexible graphite to minimize the yield of sputtered material. Lab power supplies and a lab propellant feed system were used to operate the PM1R prototype model thruster. Background pressure was measured by an ionization gauge located on the tank wall adjacent to the thruster. With an 1800-V, 3.52-A beam the xenon pressure was 3.6×10^{-6} torr, applying the correction factor of 0.348 specified by the gauge manufacturer for xenon relative to nitrogen. The effective pumping speed for this condition was 2.1×10^{5} liter/s, well in excess of the roughly 1.4×10^{5} liter/s needed to ensure that the rate of ingestion of background gas was less than 1 percent of the propellant supply flow.

Figure 1 shows the main features of the thrust stand, consisting of a standard pendulum with a hardened steel knife edge pivot, counterweight, high precision inclinometer (Rieker Electronics model SB1U), and eddy current damper. The pivot is shown more clearly in Figure 2, and the gas and electrical connections are shown in Figure 3. Electrical power was carried by highly flexible, finely stranded, PVC insulated 22 AWG wires. Multiple wires were used so that the maximum current per wire was 1.75 A. The eddy current damper consisted of an aluminum plate suspended below the thruster on an aluminum rod. The plate swung through the gap between the 2 in. high by 4 in. wide (5.1- by 10.2-cm) poles of a permanent magnet assembly consisting of two pairs of NdFeB magnets. The damping force was enhanced by arranging the pairs (design by Dura Magnetics, Inc.) to produce a field reversal at the center of the assembly. By experimentation it was found that a 0.025 in. (0.64 mm) thick aluminum plate provided nearly critical damping at a gap such that the maximum magnetic field magnitude at the center of the gap was 0.33 T. Perhaps due to the action of the damper, there was no detectable effect of facility vibration on the output of the inclinometer or load cell.

The load cell (Transducer Techniques GSO-30) was mounted to a translation stage and connected to the back of the thruster, at thruster centerline, by a length of 50-lb test braided fishing line (Fig. 4). Thrust was measured by translating the load cell until the tension in the line exceeded the anticipated thrust. This was done while running the neutralizer and main discharge, but without ion beam extraction ("discharge only" mode). The difference in line tension created by energizing the grids yielded a measurement of thrust due to ion beam extraction. Multiple measurements were obtained in relatively short time by cycling the grid voltages. This strategy sought to minimize thermal drift of the thrust stand by obtaining prompt readings (typically, the switching transient died out within 10 to 15 sec, and a steady reading was recorded for 1 to 2 min), and by minimizing the change in currents and power to the thruster.

The load cell sensitivity was not adequate to accurately measure thrust in "discharge only" mode, or with cold flow alone. However, by adjustment of the counterweights it was possible to obtain those measurements using the inclinometer.

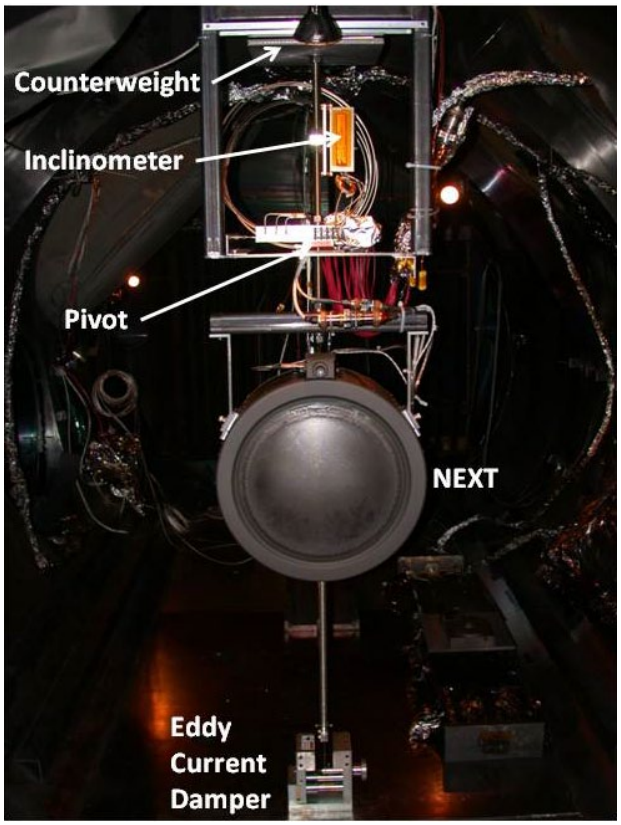

Figure 1.—Thrust stand.

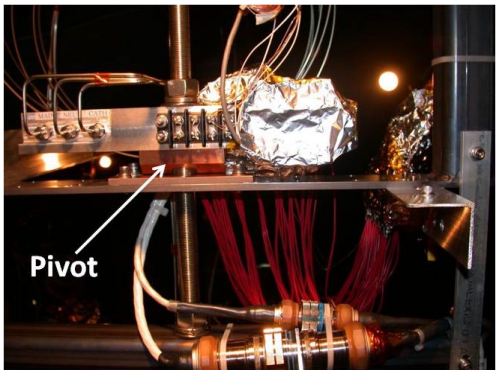

Figure 2.—Pivot.

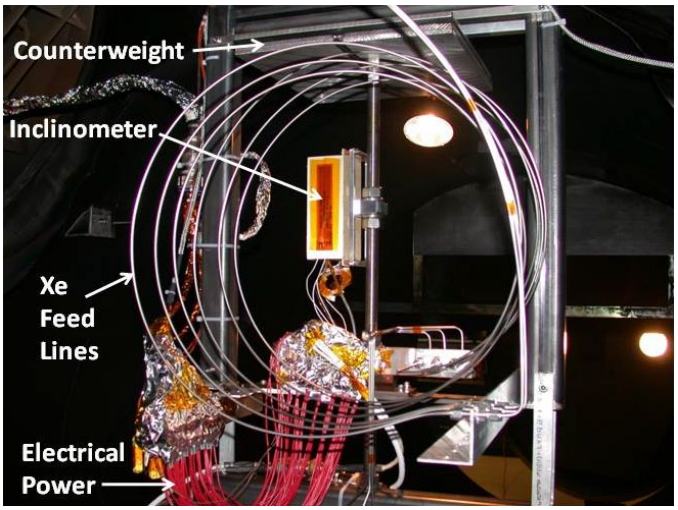

Figure 3.—Propellant and electrical connections.

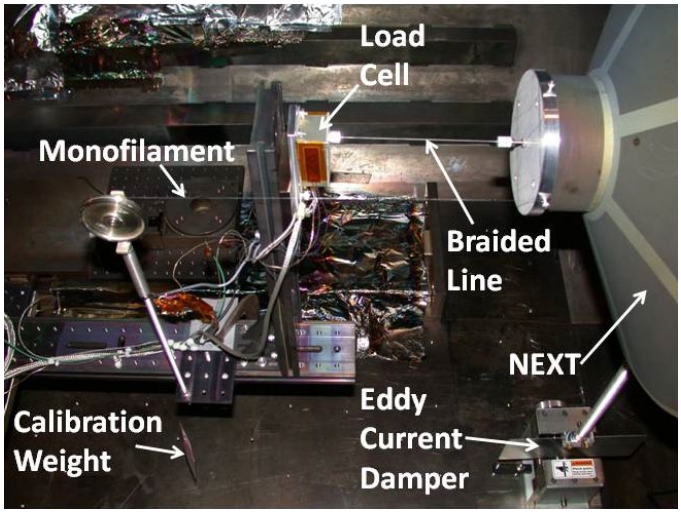

Figure 4.—Thrust stand operation with load cell.

3.0 Analysis and Calibration

The diagram shown in Figure 5 was used to determine the relations needed to reduce the raw data for thrust due to ion beam extraction. The pendulum is shown inclined by an angle θ (positive sense as shown) from the vertical. The mass distributed above the pivot (m_{cw}) is assumed to be concentrated at some location that we will call the counterweight center of mass, and that below (m_T) at a location we will call the thruster center of mass. The blue line represents the braided line connecting the load cell (marked "s" for "sensor") to a stud protruding from the back of the thruster, on thruster centerline. The red line represents a monofilament connecting the thruster to a calibration weight strung over a pulley. The location of the top of the pulley is marked "c" (for "calibration") and the point of attachment to the thruster is at the height of the thruster centerline, but offset in the horizontal plane (Fig. 4). The thrust stand is insensitive to such an offset.

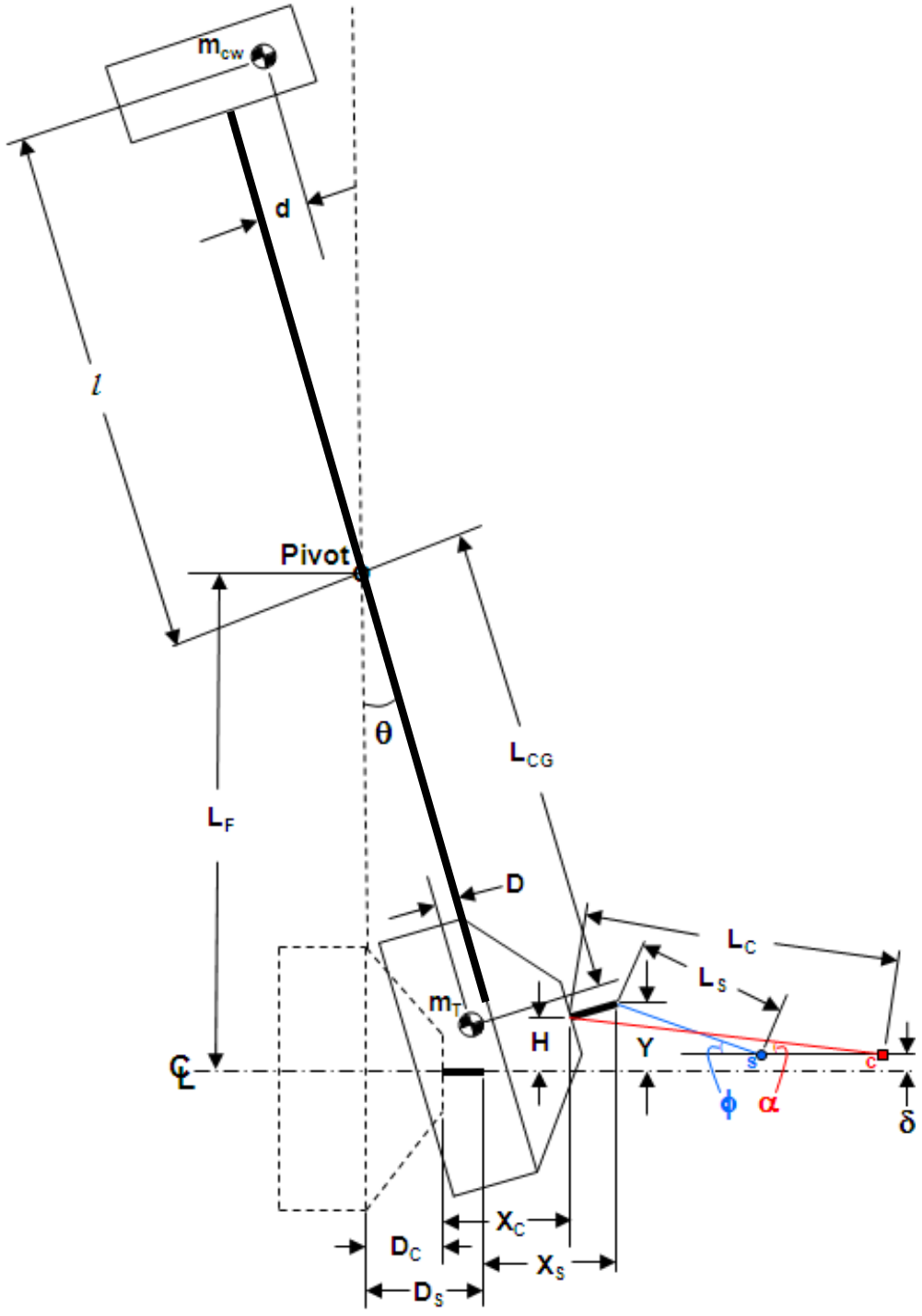

Figure 5.—Measurement schematic.

For thrust measurements the monofilament was absent, and summing moments about the pivot (at steady state, $\dot{\theta} = \ddot{\theta} = 0$) yields:

$$F_T L_F + F_S (L_F - Y)\cos\phi - F_S (X_S + D_S)\sin\phi \\ -m_T g(L_{CG}\sin\theta - D\cos\theta) + m_{CW} g(l\sin\theta - d\cos\theta) + \Sigma M_e = 0 \tag{1}$$

where F_T is thrust, assumed to act normal to the grid surface at thruster centerline, F_S is the tension in the braided line, ΣM_e represents moments due to the gas and electrical connections, and g is the acceleration due to gravity at sea level. The counterweight was set so that the magnitudes of θ and ϕ were at most 0.5 and 1.5° respectively, and the small angle approximations ($\cos\phi = \cos\theta = 1$, $\sin\phi = \phi$, $\sin\theta = \theta$) are valid. If we further neglect terms that are second order in θ, and neglect $\delta L_F\theta$ relative to δD_S (δ is the vertical offset between the load cell and thruster centerline), Equation (1) becomes:

$$F_T + F_S\left[1 + \frac{\delta D_S}{L_S L_F} - \frac{D_S}{L_F}\theta\left(1 + \frac{D_S}{L_S}\right)\right] - \frac{1}{L_F}\left[m_T g(L_{CG}\theta - D) - m_{CW} g(l\theta - d) - \Sigma M_e\right] = 0 \tag{2}$$

δ is nominally zero, and will be important only in the uncertainty analysis.

F_T was determined by writing Equation (2) once with ion beam extraction, once without, and subtracting. This procedure would have been relatively simpler if the inclination, θ, was constant with and without ion beam extraction. In practice it was found to vary by a very small amount (0.002° to 0.013°), but large enough to require inclusion in the analysis. This variation, corresponding to linear displacements from approximately 7.7×10^{-4} to 5.0×10^{-3} in. (0.02 to 0.13 mm), arose roughly in equal parts from stretch in the braided line and in the strain-gauge based load cell. In any case, subtraction of Equation (2) with beam extraction from Equation (2) without beam extraction yields:

$$F_T = \Delta F_S\left[1 + \frac{\delta D_S}{L_S L_F} - \frac{D_S}{L_F}\theta_{avg}\left(1 + \frac{D_S}{L_S}\right)\right] - g\left(m_T\frac{L_{CG}}{L_F} - m_{CW}\frac{l}{L_F}\right)\Delta\theta \tag{3}$$

where Δ indicates a difference in two readings, θ_{avg} is the average inclination, and ΣM_e is assumed constant over the very small variation in θ. In order to arrive at this form it was necessary to assume the following:

$$\frac{D_S}{2}(F_{S1} + F_{S2})\left(1 + \frac{D_S}{L_S}\right) << g(m_T L_{CG} - m_{CW} l) \tag{4}$$

where F_{S1} and F_{S2} are readings with and without beam extraction respectively. The validity of this assumption will be demonstrated shortly.

Equation (3) shows that in addition to load cell and inclinometer calibrations, knowledge of the mass properties of the pendulum was needed to calculate thrust. The arrangement shown in Figure 4 was used, at ambient conditions, to calibrate the mass properties. Simulating a thrust measurement, the load cell was translated to produce tensions in the braided line slightly in excess of the desired simulated thrusts, then weights were hung from the monofilament line, relieving tension in the braided line. With reference to Figure 5, summing moments about the pivot at steady state yields:

$$F_C(L_F - H)\cos\alpha - F_C(D_C + X_C)\sin\alpha + F_S(L_F - Y)\cos\phi - F_S(X_S + D_S)\sin\phi \\ -m_T g(L_{CG}\sin\theta - D\cos\theta) + m_{CW} g(l\sin\theta - d\cos\theta) + \Sigma M_e = 0 \tag{5}$$

where F_C is the tension in the monofilament line. After applying the small angle approximations (magnitude of α was less than 0.5°), neglecting terms that are second order in θ, and neglecting $\delta L_F \theta$ relative to δD_S and δD_C, Equation (5) becomes:

$$F_C\left[1+\frac{\delta D_C}{L_C L_F}-\frac{D_C}{L_F}\theta\left(1+\frac{D_C}{L_C}\right)\right]+F_S\left[1+\frac{\delta D_S}{L_S L_F}-\frac{D_S}{L_F}\theta\left(1+\frac{D_S}{L_S}\right)\right] \\ -\frac{1}{L_F}\left[m_T g\left(L_{CG}\theta-D\right)-m_{CW} g\left(l\theta-d\right)-\Sigma M_e\right]=0 \tag{6}$$

As before, we write Equation (6) twice and subtract, yielding:

$$g\left(m_T\frac{L_{CG}}{L_F}-m_{CW}\frac{l}{L_F}\right) \\ =\frac{1}{\Delta\theta}\left\{\Delta F_C\left[1+\frac{\delta D_C}{L_C L_F}-\frac{D_C}{L_F}\theta_{avg}\left(1+\frac{D_C}{L_C}\right)\right]+\Delta F_S\left[1+\frac{\delta D_S}{L_S L_F}-\frac{D_S}{L_F}\theta_{avg}\left(1+\frac{D_S}{L_S}\right)\right]\right\} \tag{7}$$

To arrive at this form it was necessary to assume:

$$\frac{D_C}{2}\left(F_{C1}+F_{C2}\right)\left(1+\frac{D_C}{L_C}\right)\approx\frac{D_S}{2}\left(F_{S1}+F_{S2}\right)\left(1+\frac{D_S}{L_S}\right)<<g\left(m_T L_{CG}-m_{CW} l\right) \tag{8}$$

The right hand side (RHS) of Equation (7) involves the difference (ΔF_C and ΔF_S are of opposite sign) of two nearly equal numbers, resulting in large uncertainty in the calculated mass properties. Therefore, 84 measurements were averaged, yielding a value of 8.6×10^3 mN for the left hand side (LHS) of Equation (7), and thereby a value of 4.8×10^5 mN-cm for the RHS of Equation (8) (L_F = 56.4 cm). The LHSs of Equation (8) have a maximum value of 3.8×10^3, validating Equations (4) and (8).

The inclinometer was calibrated under vacuum, with the thruster operating, by displacing the thruster known amounts using a rod attached to a linear translation stage. The load cell was calibrated (Fig. 6) at ambient conditions with a series of 7 weights ranging from 2.5 to 24.5 g (24.6 to 241 mN), spanning the nominal throttle table thrust range (25.6 to 236.4 mN). The load cell and inclinometer were heated and controlled to their ambient operating temperatures while under vacuum.

Calibration for cold flow and "discharge only" thrust measurements was performed under vacuum with the set-up shown in Figure 7. This is the familiar arrangement in which a series of weights was lowered by a motor over a pulley and the response of the stand (in this case a change in inclination) was recorded. Ten 51 mg washers were used as calibration weights.

4.0 Results

4.1 Discharge Only, Cold Flow

We will attempt to model the thrust produced by the neutral gas flowing from the discharge chamber of an ion thruster under the condition of zero input power using an expression of the form:

$$F_{cf}=C_{cf}\dot{m}_d\bar{c}, \tag{9}$$

where F_{cf} is the cold flow thrust, C_{cf} is a factor that accounts for off-axis flow, $\dot{m}_d$ is the discharge chamber mass flow rate, and $\bar{c}$ is the mean thermal speed of the neutrals, given by:

$$\bar{c} = \sqrt{\frac{8kT_n}{\pi m_n}}, \tag{10}$$

where k is Boltzmann's constant, T_n is the neutral gas temperature, and m_n is the gas molecular mass.

Figure 6.—Load cell calibration.

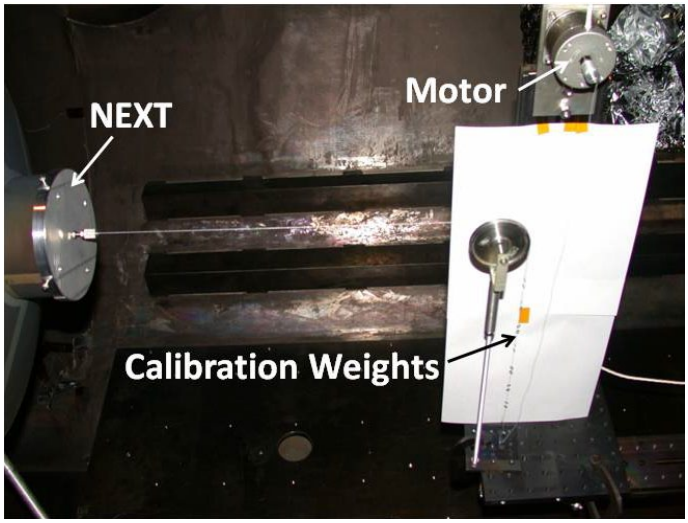

Figure 7.—Calibration for cold flow and discharge only thrust measurements.

Ion thruster discharge chambers operate within the free molecular flow regime. For the case of flow through thin-walled apertures, the cosine law of molecular effusion applies (Ref. 21). In the case of a flat grid we obtain:

$$C_{cf} = \frac{\int_0^{\frac{\pi}{2}} \cos^2(\varepsilon)\sin(\varepsilon)d\varepsilon}{\int_0^{\frac{\pi}{2}} \cos(\varepsilon)\sin(\varepsilon)d\varepsilon} \tag{11}$$

where ε is the angle relative to aperture centerline. This expression integrates to the simple result: $C_{cf} = 2/3$.

A more realistic analysis must account for finite aperture thickness, grid curvature, and the presence of two grids.[1] The two cylindrical apertures that a neutral particle must pass through to escape the discharge chamber present a difficult problem to model. Fortunately, Kuharski et al. modeled a two cylindrical aperture set that had a geometry that was very similar to that of the NEXT thruster (Ref. 22). They found that the angular distribution of particles exiting the accelerator grid was well modeled by assuming a single accelerator grid cylindrical aperture. This simplification was possible because of the large screen aperture diameter and low thickness relative to that of the accelerator grid. This same simplifying assumption will be exploited here.

Clausing was the first to develop an expression for the angular distribution of particles downstream of a cylindrical aperture (Ref. 23). His equation assumes that the aperture is a point source and that the flux of particles from the walls of the aperture is linear as a function of axial thickness, which is a very accurate assumption over a range of aperture thickness-to-radius ratios that span from 0 to about 8 (Ref. 24). The angular distribution of particles downstream of a cylindrical aperture, $T_c(\varepsilon)$, in the far-field is given by (Refs. 23 and 25):

$$T_c(\varepsilon) = \begin{cases} -\left\{\frac{2}{\pi}(1-\kappa)\left[\arcsin\left(\frac{t\tan(\varepsilon)}{2R}\right) + \frac{t\tan(\varepsilon)}{2R}\sqrt{1-\left(\frac{t\tan(\varepsilon)}{2R}\right)^2}\right]\right\} \\ \qquad + \frac{4}{3\pi}(1-2\kappa)\frac{1-\left[1-\left(\frac{t\tan(\varepsilon)}{2R}\right)^2\right]^{\frac{3}{2}}}{\frac{t\tan(\varepsilon)}{2R}} \quad \text{if } \varepsilon \le \arctan\left(\frac{2R}{t}\right) \\ \text{and} \\ \kappa + \frac{4}{3\pi}\frac{1-2\kappa}{\frac{t\tan(\varepsilon)}{2R}} \quad \text{if } \varepsilon > \arctan\left(\frac{2R}{t}\right) \end{cases} \tag{12}$$

where:

$$\kappa = \frac{\sqrt{t^2+4R^2}-t}{2R + \frac{4R^2}{\sqrt{t^2+4R^2}}} \tag{13}$$

[1] Analysis by George Soulas.

Here, t is the accelerator aperture thickness, ε is the angle that the velocity makes with the aperture centerline, and R is the accelerator grid aperture radius. The contribution to C_{cf} from a single aperture is obtained from:

$$C_{cf,hole} = \frac{\int_0^{\frac{\pi}{2}} T_c(\varepsilon)\cos^2(\varepsilon)\sin(\varepsilon)d\varepsilon}{\int_0^{\frac{\pi}{2}} T_c(\varepsilon)\cos(\varepsilon)\sin(\varepsilon)d\varepsilon} \tag{14}$$

The total C_{cf} can be found by correcting the contribution per hole for off-axis thrusting due to grid curvature:

$$C_{cf} = C_{cf,hole}\frac{\int_0^{\psi_{max}} \cos(\psi)\sin(\psi)d\psi}{\int_0^{\psi_{max}} \sin(\psi)d\psi} \tag{15}$$

where ψ is the angle from grid centerline and ψ_{max} is the angle to the edge of the accelerator grid perforated pattern. This analysis assumes that the upstream neutral density is uniform over the grid. For a NEXT accelerator grid, the correction factor C_{cf} is found to be 0.720.

Measured values of cold flow "discharge only" thrust (no flow to the neutralizer) are shown in Figure 8. These measurements were obtained by cycling the flow on and off and noting the change in thrust stand inclination. Six readings were taken and averaged at each flow rate. The selected flow rates correspond to thrust levels (TLs) 12, 27, and 40. Measurements were taken after the thruster sat under steady vacuum conditions overnight and prior to the application of any electrical power. The thrust stand frame temperature was –11 °C, and this was taken to be the temperature of the thruster, and of the neutral gas. By including the point (0,0) and fitting the data to a straight line, we obtain $C_{cf} = 0.74$.

4.2 Neutralizer Only

Neutralizer thrust was measured (again by cycling on and off) for the case of warm neutral flow (heater at the ignition current level, but no plasma) and for a 3 A keeper discharge. The measurements include a correction factor of 2.0 to account for the difference between the neutralizer-to-pivot moment arm and that between the point of application of the calibration weights (thruster centerline) and the pivot. We will attempt to model both cases using a continuum fluid approach (neutralizer internal pressure ~ O(10) Torr), and will consider a purely thermal thrust mechanism, for which thrust can be estimated from:

$$F_n = \dot{m}_n u_e + p_e A_e \tag{16}$$

where F_n is the neutralizer thrust, $\dot{m}_n$ is the neutralizer flow rate, u_e is the effective exhaust velocity, p_e is the pressure at the neutralizer exit aperture, and A_e is the exit aperture area (ambient pressure is assumed to be negligible). If we assume an isentropic expansion to Mach number = 1 at the exit plane, we obtain:

$$F_n = \dot{m}_n\sqrt{kRT_o}\left(\frac{2}{k+1}\right)^{1/2}\left(1+\frac{1}{k}\right) \tag{17}$$

where k is the ratio of specific heats, R is the specific gas constant, and T_o is the gas stagnation temperature.

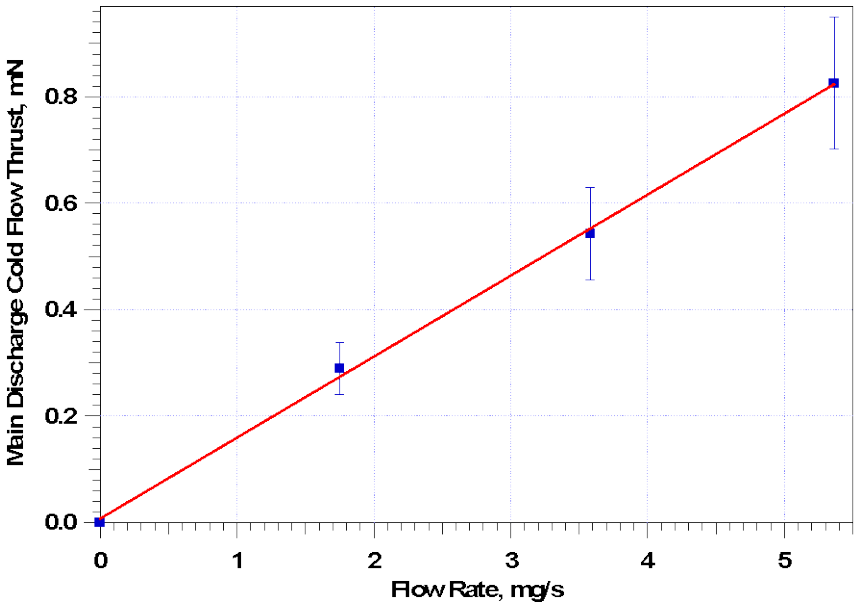

Figure 8.—Discharge only cold flow thrust, temperature = –11 °C.

For the warm flow case, at a xenon flow rate of 10 sccm and assumed stagnation temperature of 1100 °C, Equation (17) yields a predicted thrust of 0.52 mN. The measured value at 10 sccm (average of 5 measurements) was also 0.52 mN, with an estimated uncertainty of 16 percent. 10 sccm is a larger than nominal neutralizer flow, and was selected to improve the measurement signal-to-noise ratio without any expectation of altering the physics.

For the case of a 3 A keeper discharge (heater turned off), the flow rate was 6 sccm, and the measured thrust (average of 6 measurements) was 0.41 mN with an estimated uncertainty of 18 percent. At F_n = 0.41 mN and $\dot{m}_n$ = 6 sccm, Equation (17) yields a prediction of 2360 °K for T_o. Neutral temperatures near this value have been experimentally observed (Ref. 26) and predicted by numerical simulation (Refs. 27 and 28) in the region near the exit aperture of a hollow cathode.

4.3 Discharge Only with Plasma

Thrust was measured with power supplied to the main discharge chamber, but with the screen and accelerator grid power supplies turned off. The neutralizer ran continuously at 6 sccm with a 3 A keeper discharge during this experiment, while the main discharge (power and flow) was cycled on and off to determine its contribution to thrust. Main discharge run times were kept short (less than 1 min) to minimize heating of the thrust stand in an attempt to avoid thermal drifting. Nevertheless, thermal drifting was observed to be significant on the time scale of the measurements, probably as a result of changes in electrical cable tension. The contribution to the change in thrust stand inclination due to the cables was estimated in the following way. Following shut-down of the main discharge power and flow, the rate of change of thrust stand inclination with time was determined at a point at which the gas flow had diminished to 5 to 10 percent of its steady value, as determined by vacuum chamber pressure readings (thrust assumed to be negligible at that point). This rate was assumed to apply during the period of thrust cessation, and was multiplied by the time required to get to 5 to 10 percent of steady flow to obtain the contribution from the cables. This was then subtracted from the total inclination change over that same period to obtain the main discharge contribution. In our error analysis we arbitrarily assigned an uncertainty of 50 percent to the inclination change due to the cables.

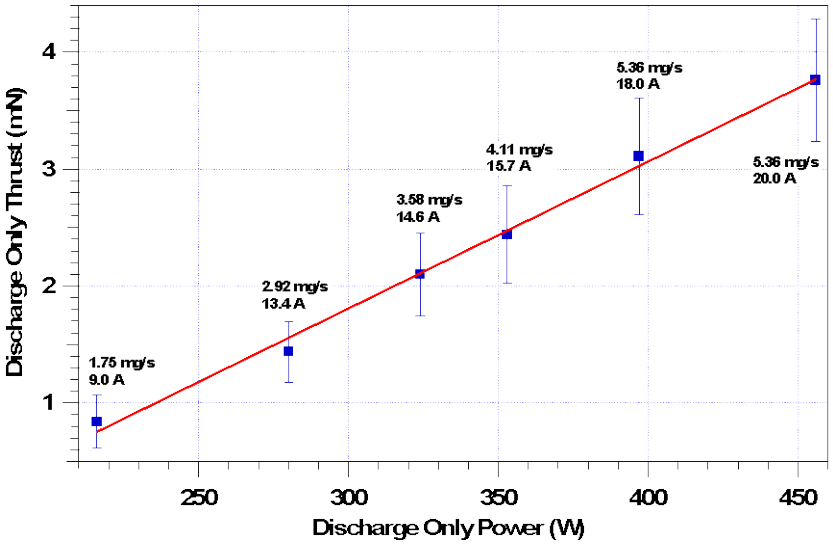

Figure 9.—Discharge only thrust, discharge mass flow and current listed by each data point.

Results are shown in Figure 9 for a range of "discharge only" power levels spanning those found in the nominal throttle table. Flow rates and discharge currents are listed with each data point. Each point represents the average of 2 to 5 measurements. It is evident that thrust scales linearly with discharge power, and that the values are significantly greater than those found with cold flow (Fig. 8). If we assume that thrust is generated by the escape of thermal neutrals and apply the analysis from Section 4.1 (with $C_{cf} = 0.74$), we find that neutral temperatures from 2100 to 5600 °K are required. This finding conflicts with the common assumption that the neutral gas accommodates to the thruster operating temperature (Ref. 29), which for NEXT does not exceed approximately 530 °K in the steady state (Ref. 30). Nevertheless, this mechanism appears to be plausible since ion temperatures from approximately 5000 to 15000 °K have been measured in an ion thruster discharge chamber at a discharge power of 325 W (Ref. 31). Hot neutrals could be created by Xe^+-Xe elastic or charge exchange collisions. We estimate the mean free paths for these processes to be 5 to 6 cm (Refs. 32 and 33), considerably smaller than NEXT discharge chamber dimensions.

Other non-thermal mechanisms appear to be less plausible. With the screen and accelerator grid power supplies off, the anode and accelerator grid are at the same potential (the screen supply is tied between the anode and neutralizer, and the accelerator supply is referenced to the neutralizer), and ions created near anode potential are unlikely to escape. High energy neutrals can be produced by charge exchange with ions accelerating through the sheath upstream of the screen grid, but with Debye lengths on the order of 0.01 to 0.1 mm (Ref. 34), sheath thickness on the order of 10 Debye lengths (Ref. 35), and estimated charge exchange mean free paths on the order of 10 cm for a 25 eV ion, this mechanism is estimated to account for less than 10 percent of the observed thrust. Ions created in the vicinity of the cathode with energies (relative to the cathode) in excess of the discharge voltage could escape directly, or do so as neutrals following charge exchange collisions, however for cathodes studied in simulated discharge chamber environments those ions tend not to be axially directed (Refs. 36 to 38).

4.4 Ion Beam

Thrust due to ion beam extraction was measured for the complete 40-level throttle table by the load cell method described in Sections 2.0 and 3.0. Sample raw data (6 on-off cycles) from thrust level (TL) 32 are shown in Figure 10. Six measurements were taken at each TL, with the exception of TLs 5, 9, 13, and 18, for which 11, 18, 7, and 7 measurements were taken respectively. The neutralizer ran continuously at 6 sccm with a 3 A keeper discharge during this experiment. The thruster was warmed up daily prior to data collection by operating at either TL5 or TL9 for 3.5 to 4 hr, or at TL37 for 2 to 2.5 hr.

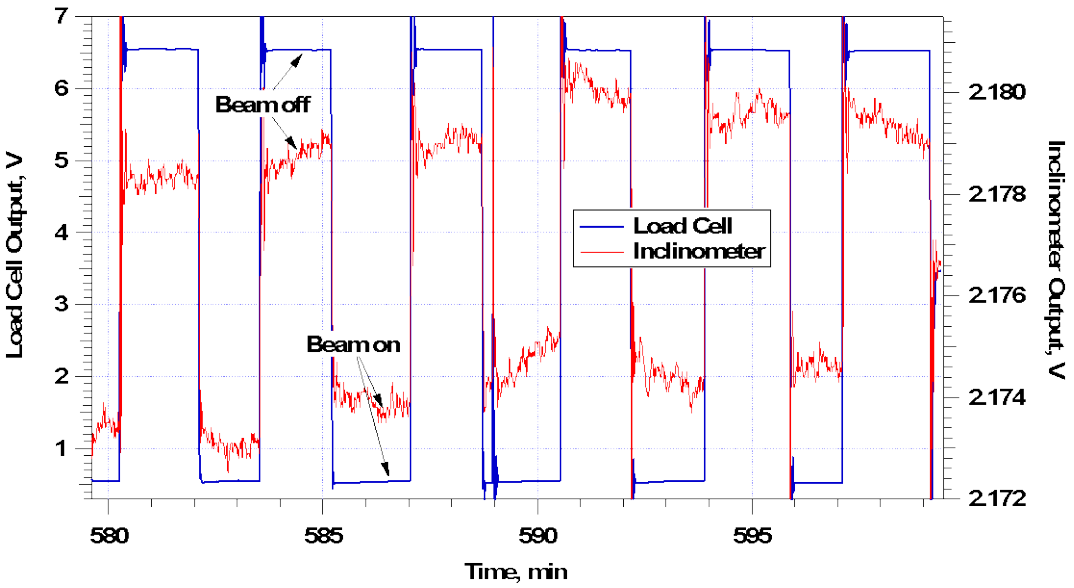

Figure 10.—Sample ion beam thrust measurement raw data, TL32.

Table 1 lists typical values and uncertainties for the parameters involved in data reduction. The quoted uncertainties for the various lengths (except δ) reflect the practical difficulty of making measurements on and around the thruster. The uncertainty in δ is the displacement observed to occur as a result of vacuum-atmosphere cycling on the facility. Noise on the inclinometer output determined the uncertainties in ϑ_{avg} and $\Delta\vartheta$, and that in ΔF_C was determined by the accuracy of the scale used to weigh the calibration weights. The results of the load cell calibration (ΔF_S) show an average uncertainty of 0.14 percent over the tested range (24.6 to 241 mN). Thrust uncertainty was dominated by terms containing δ, a situation which, in hindsight, could have been most easily avoided by using a longer braided line.

TABLE 1.—VALUES FOR UNCERTAINTY ANALYSIS

Parameter	Typical value	Absolute uncertainty	Percentage uncertainty
L_F (cm)	56.4	0.25	-----
L_C (cm)	38.9	0.25	-----
L_S (cm)	14.6	0.25	-----
D_C (cm)	24.4	0.25	-----
D_S (cm)	28.2	0.25	-----
ϑ_{avg} (deg)	–0.4 to 0.8	0.0008	-----
$\Delta\vartheta$ (deg)	0.002 to 0.015	0.0008	-----
δ (cm)	0	0.13	-----
ΔF_C (mN)	24 to 240	0.001	-----
ΔF_S (mN)	24 to 240		0.14

4.5 Total Thrust

Total thrust was calculated by summing the contributions from ion beam extraction (Section 4.4), the main discharge without beam extraction (Section 4.3), and the neutralizer without beam extraction (Section 4.2). Main “discharge only” thrust was determined by applying the linear fit shown in Figure 9 to measured “discharge only” power at each TL. No attempt was made to apply a correction for the fact that the discharge chamber was not at a steady state temperature during the measurements of discharge only thrust. This is rationalized by our conjecture (Section 4.3) that the neutral temperature in the main body of the discharge is not governed by the thruster operating temperature.

Table 2 contains the results ($F_{measured}$) for the 40 NEXT throttle levels, along with comparisons to the nominal NASA Throttle Table 10 (F_{TT10}), and to TT10 with values corrected with plume data recently acquired at The Aerospace Corporation (Ref. 2) (Corrected F_{TT10}). $F_{measured}$ represents measurement averages, and σ is the measurement standard deviation. V_{bps} is the beam power supply (screen supply) voltage. Standard methods for propagating uncertainties (Ref. 39) were employed to arrive at the values shown in the final column of Table 2.

TABLE 2.—THRUST COMPARISON

TL	V_{bps} (V)	$F_{measured}$ (mN)	F_{TT10} (mN)	Corrected F_{TT10} (mN)	$F_{measured} - F_{TT10}$ (%)	$F_{measured}$ – corrected F_{TT10} (%)	$\sigma/F_{measured}$ (%)	$F_{measured}$ uncertainty (%)
m_d = 1.56 mg/s, J_b = 1.00 A								
1	275	25.4	25.6	25.4	–0.8	–0.3	0.2	1.1
m_d = 1.75 mg/s, J_b = 1.20 A								
2	300	31.4	31.9	31.5	–1.6	–0.5	0.6	1.2
3	400	37.1	37.2	37.0	–0.4	0.4	0.5	1.2
4	650	47.9	48.2	47.7	–0.5	0.5	0.2	1.0
5	679	49.1	49.2	48.9	–0.2	0.5	0.3	1.1
6	850	54.5	55.2	54.6	–1.2	–0.2	0.2	0.9
7	936	56.9	57.9	57.1	–1.7	–0.3	0.2	0.9
8	1021	59.2	60.5	59.6	–2.1	–0.6	0.2	0.8
9	1179	63.4	65.1	63.9	–2.5	–0.7	0.2	0.8
10	1396	68.8	70.8	69.5	–2.8	–0.9	0.2	0.8
11	1567	72.9	75.1	73.7	–2.9	–1.1	0.1	0.7
12	1800	77.9	80.3	78.8	–3.1	–1.2	0.1	0.7
m_d = 2.33 mg/s, J_b = 1.60 A								
13	1021	79.6	80.6	79.4	–1.3	0.3	0.2	0.8
14	1179	85.1	86.8	85.3	–2.0	–0.2	0.0	0.8
15	1396	92.3	94.5	92.8	–2.3	–0.6	0.1	0.7
16	1567	97.7	100.1	98.4	–2.5	–0.8	0.3	0.6
17	1800	104.4	107.0	105.2	–2.5	–0.8	0.1	0.6
m_d = 2.92 mg/s, J_b = 2.00 A								
18	1021	100.3	100.7	99.5	–0.4	0.8	0.2	0.8
19	1179	107.0	108.4	106.7	–1.2	0.3	0.1	0.8
20	1396	115.9	117.9	115.9	–1.7	0.0	0.1	0.7
21	1567	122.6	125.0	122.9	–1.9	–0.3	0.3	0.7
22	1800	130.9	133.9	131.8	–2.3	–0.6	0.1	0.7
m_d = 3.58 mg/s, J_b = 2.35 A								
23	1021	118.9	118.9	118.1	0.0	0.7	0.1	0.8
24	1179	127.0	128.0	126.5	–0.8	0.3	0.2	0.7
25	1396	137.4	139.4	137.6	–1.4	–0.1	0.1	0.7
26	1567	145.2	147.5	145.6	–1.6	–0.2	0.1	0.7
27	1800	155.2	157.9	155.8	–1.7	–0.4	0.2	0.7
m_d = 4.11 mg/s, J_b = 2.70 A								
28	1021	137.1	136.6	135.8	0.4	1.0	0.2	0.8
29	1179	146.4	146.9	145.4	–0.4	0.7	0.1	0.7
30	1396	158.5	160.0	157.9	–0.9	0.4	0.1	0.7
31	1567	167.1	169.4	167.1	–1.4	0.0	0.1	0.7
32	1800	178.4	181.4	178.9	–1.6	–0.3	0.1	0.7
m_d = 4.72 mg/s, J_b = 3.10 A								
33	1179	168.6	168.7	167.2	–0.1	0.9	0.1	0.7
34	1396	182.5	183.7	181.4	–0.6	0.6	0.1	0.7
35	1567	192.6	194.4	191.8	–0.9	0.4	0.1	0.7
36	1800	205.5	208.4	205.5	–1.4	0.0	0.0	0.7
m_d = 5.36 mg/s, J_b = 3.52 A								
37	1179	192.4	191.8	190.2	0.3	1.2	0.1	0.7
38	1396	208.0	208.8	206.4	–0.4	0.8	0.2	0.7
39	1567	219.4	220.7	217.9	–0.6	0.7	0.1	0.7
40	1800	234.6	236.9	233.6	–1.0	0.4	0.1	0.7

We should note that in our comparison to the TT10 values, the neutralizer thrust contribution is applied in an approximate manner. The neutralizer flow rate of 6 sccm differs from the nominal TT10 values, which range from 2.5 to 4.0 sccm (6 sccm was chosen to ensure that the keeper discharge would not extinguish during extended periods with no ion beam extraction). Also, the change in neutralizer thrust between operation with and without ion beam extraction was only partially captured (due to the smaller neutralizer-pivot moment arm) by the measurements from Section 4.4. Fortunately, neutralizer thrust is small, and these inaccuracies are likely to fall within the quoted total thrust measurement uncertainties.

The data from Table 2 are plotted in Figure 11. The structure in the "difference" traces is nearly identical in form to that of the thrust correction factor due to beam divergence (β) calculated from plume data recorded at The Aerospace Corporation (Fig. 12). This implies a proportionality between the two, and suggests the need for additional plume measurements to improve the fidelity of β. Another explanation for the difference trace structure which seems less probable (because it doesn't explain TLs 2-5) is that the true ion beam current was reduced due to backstreaming of plume electrons to the anode. Backstreaming, possibly through the perforated ground screen, is favored by increasing beam supply voltage.

Figure 13 compares thrust correction factors (γ) obtained from thrust stand measurements to those derived from plume current density and charge-state measurements made at The Aerospace Corporation (Ref. 2), and to the NASA TT10 values. γ accounts for thrust losses due to beam divergence and multiply-charged ions, and is defined by the well-known expression for the thrust F of an ion engine:

$$F = \gamma J_b \sqrt{2mV_b/q} \tag{18}$$

where J_b is the ion beam current, V_b is the ion beam voltage (not equal to V_{bps}), m is the ion mass, and q is the elementary charge. The V_b values needed to calculate γ from thrust stand measurements were obtained from the NASA TT10. Plotting γ allows us to observe that the error bars for the thrust stand derived values and those calculated from plume data overlap for the entire throttle table with the exception of TL37. This is remarkably good agreement for measurements made by independent methods.

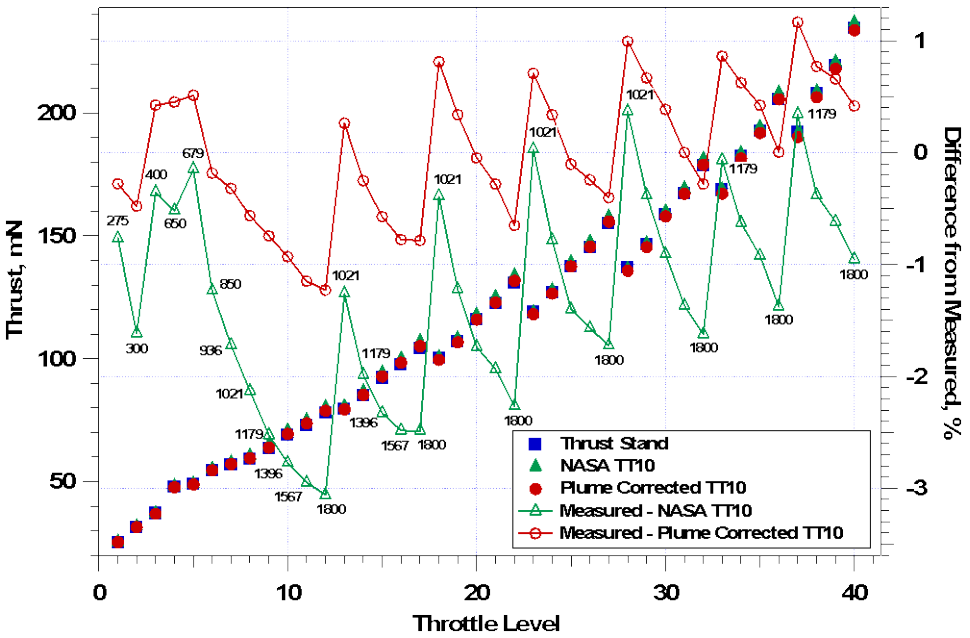

Figure 11.—Measured and predicted total thrust (from Table 2, solid symbols). Error bars in measured thrust are smaller than the symbols. "Difference" traces shown with lines and open symbols. "Measured— NASATT10" trace annotated with beam power supply voltages.

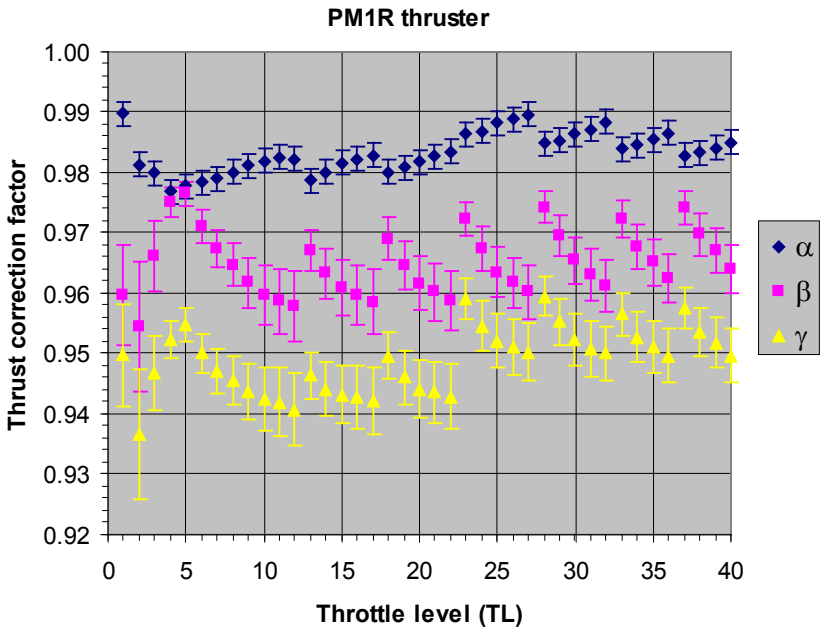

Figure 12.—PM1R thrust correction factors (calculated from plume data) for doubly-charged ions α, beam divergence β, and their product γ versus throttle level (from Ref. 2).

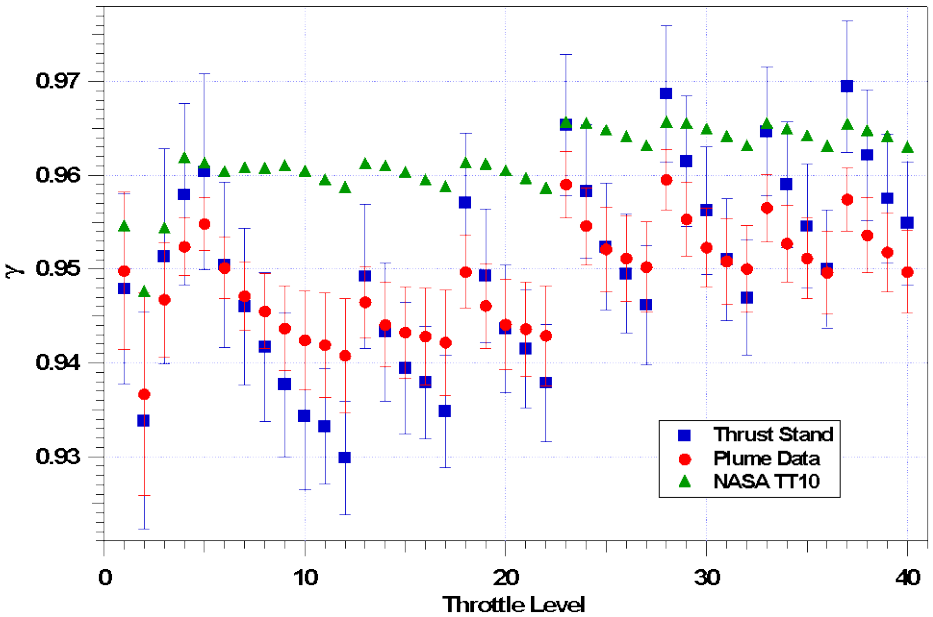

Figure 13.—Thrust correction factors from the nominal NASA TT10, calculated from plume ion flux and charge state measurements (Ref. 2), and calculated from direct thrust measurements.

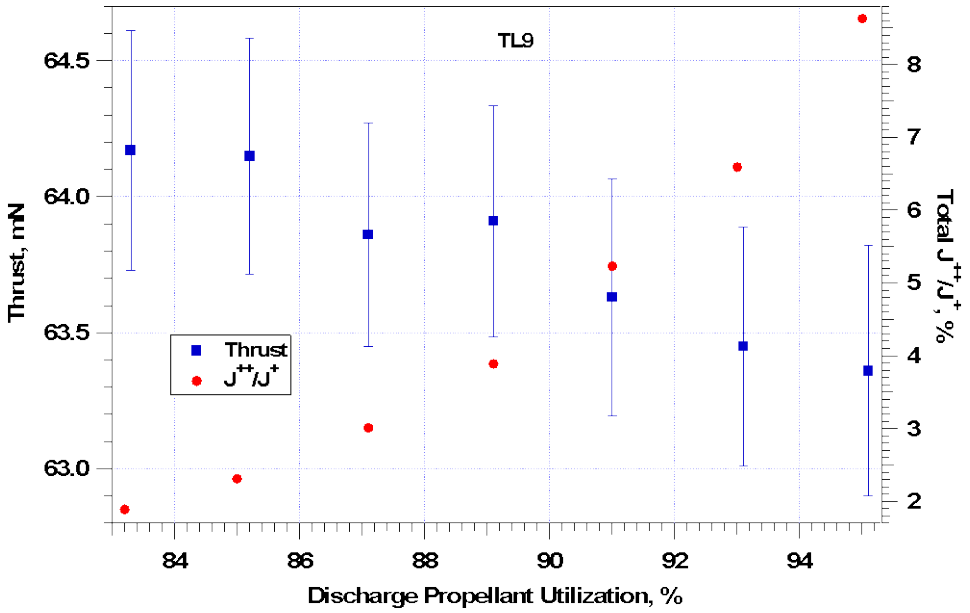

Figure 14.—Thrust and total J^{++}/J^{+} (J^{++}/J^{+} from Ref. 2) versus utilization at TL9.

Figure 14 shows measured thrust as a function of discharge chamber propellant utilization (ratio of ion beam current to discharge chamber mass flow expressed in equivalent amperes) for TL9 (nominal discharge propellant utilization for TL9 is 93 percent). Declining thrust with increasing utilization is consistent with data from Reference 2 which show that the total doubly ionized current fraction (J^{++}/J^{+}) increases from approximately 2 to 9 percent over the same range of utilization.

5.0 Conclusion

Direct thrust measurements have been made on the NASA NEXT ion engine and compared to the NASA throttle table 10 (TT10) for the full set of 40 throttle levels (TLs), as well as for a few off-nominal operating conditions. Measurements differ from the nominal TT10 values by 3.1 percent at most, while at 30 TLs the difference is less than 2.0 percent. When measurements are compared to the TT10 values corrected with ion beam current density and charge state data obtained at The Aerospace Corporation, they differ by 1.2 percent at most, and by 1.0 percent or less at 37 TLs. Comparison of thrust correction factors (γ) calculated from direct thrust measurements to those calculated from The Aerospace Corporation's plume data agree to within measurement error for all but one of the throttle levels.

Measurements of cold flow thrust and thrust with plasma present but without ion beam extraction have been made for the main discharge and neutralizer. In all cases thrust is postulated to arise from the escape of thermal neutrals, and analytical expressions are given that allow accurate thrust estimation if the neutral gas temperature is known.

References

1. Crofton, M.W., Pollard, J.E., Beiting, E.J., Spektor, R., Diamant, K.D., Eapen, X.L., Cohen, R.B., and Patterson, M.J., "Characterization of the NASA NEXT Thruster," AIAA–2009–4815, 45th Joint Propulsion Conference, Denver, CO, 2–5 Aug. 2009.
2. Pollard, J.E., Diamant, K.D., Crofton, M.W., Patterson, M.J., and Soulas, G.C., "Spatially-Resolved Beam Current and Charge-State Distributions for the NEXT Ion Engine," presented at the AIAA 46th Joint Propulsion Conference, Nashville, TN, 25–28 Jul. 2010.

3. Banks, B., Rawlin, V., Weigand, A., and Walker, J., "Direct Thrust Measurement of a 30-cm Ion Thruster," AIAA 75–340, AIAA 11th Electric Propulsion Conference, New Orleans, LA, 19–21 Mar. 1975.
4. Komurasaki, K. and Arakawa, Y., "Hall Current Ion Thruster Performance," AIAA 90–2594, AIAA 21st International Electric Propulsion Conference, Orlando, FL, Jul. 18–20, 1990.
5. Fisch, N.J., Raitses, Y., Litvak, A.A., and Dorf, L.A., "Design and Operation of Hall Thruster with Segmented Electrodes," AIAA 99–2572, 35th Joint Propulsion Conference, Los Angeles, CA, Jun. 1999.
6. Beiting, E.J., "Impulse Thrust Stand for MEMS Propulsion Systems," AIAA 99–2720, 35th Joint Propulsion Conference, Los Angeles, CA, Jun. 1999.
7. Markusic, T.E., Jones, J.E., and Cox, M.D., "Thrust Stand for Electric Propulsion Performance Evaluation," AIAA–2004–3441, 40th Joint Propulsion Conference, Fort Lauderdale, FL, Jul. 11–14, 2004.
8. Haag, T.W., "Design of a Thrust Stand for High Power Electric Propulsion Devices," AIAA 89–2829, 25th Joint Propulsion Conference, Monterey, CA, Jul. 10–12, 1989.
9. Haag, T.W. and Curran, F.M., "High Power Hydrogen Arcjet Performance," AIAA 91–2226, 27th Joint Propulsion Conference, Sacramento, CA, Jun. 24–26, 1991.
10. Welle, R.P., Pollard, J.E., Janson, S.W., Crofton, M.W., and Cohen, R.B., "One Kilowatt Hydrogen and Helium Arcjet Performance," AIAA 91–2229, 27th Joint Propulsion Conference, Sacramento, CA, Jun. 24–26, 1991.
11. Choueiri, E.Y. and Ziemer, J.K., "Quasi-Steady Magnetoplasmadynamic Thruster Performance Database," Journal of Propulsion and Power, Vol. 17, No. 5, Sep.–Oct. 2001, pp. 967–976.
12. Ziemer, J.K., "Performance Measurements Using a Sub-Micronewton Resolution Thrust Stand," 27th International Electric Propulsion Conference, Pasadena, CA, Oct. 15–19, 2001.
13. Gamero-Castano, M. and Hruby, V., "Using a Torsional Balance to Characterize Thrust at Micronewton Levels," AIAA–2003–4537, 39th Joint Propulsion Conference, Huntsville, AL, Jul. 20–23, 2003.
14. Marhold, K. and Tajmar, M., "Micronewton Thrust Balance for Indium FEEP Thrusters," AIAA–2005–4387, 41st Joint Propulsion Conference, Tucson, AZ, Jul. 10–13, 2005.
15. Brimhall, Z.N., Divitotawela, N., Atkinson, J.P., Kirk, D.R., and Peebles, H.G., "Design and Validation of a Six Degree of Freedom Rocket Motor Test Stand," AIAA–2008–5051, 44th Joint Propulsion Conference, Hartford, CT, Jul. 21–23, 2008.
16. Crofton, M.W., "Evaluation of Electric Thrusters," The Aerospace Corporation Report No. ATR–97(8201)–1, Apr. 15, 1997.
17. Brady, B.B., Coleman, D., Martin, L.R., and Lang, V.I., "Modification/Chemical Study for Replacement Propellants," The Aerospace Corporation Report No. TOR–2000(1306)–2, 17 Mar. 2000.
18. Diamant, K.D., Pollard, J.E., Cohen, R.B., Raitses, Y., and Fisch, N.J., "Segmented Electrode Hall Thruster," Journal of Propulsion and Power, Vol. 22, No. 6, Nov.–Dec. 2006, pp. 1396–1401.
19. Diamant, K.D., Zeigler, B.L., and Cohen, R.B., "Microwave Electrothermal Thruster Performance," Journal of Propulsion and Power, Vol. 23, No. 1, Jan.–Feb. 2007, pp. 27–34.
20. Diamant, K.D., Pollard, J.E., Raitses, Y., and Fisch, N.J., "Ionization, Plume Properties, and Performance of Cylindrical Hall Thrusters," IEEE Transactions on Plasma Science, Vol. 38, No. 4, Apr. 2010, pp. 1052–1057.
21. Ramsey, N.F., *Molecular Beams*, Oxford University Press, 1990, p. 13.
22. Kuharski, R.A., et al., "Ion Engine Neutralizer Erosion in Lab and Space," AIAA–2005–3880, Jul. 2005.
23. Clausing, P., "The Formation of Beams in Molecular Streaming," *Z. Physik*, Vol. 66, 1930, pp. 471–476.
24. Soulas, G.C., "Neutral Flux and Density Surrounding a Cylindrical Aperture in the Free Molecular Flow Regime," to be published as a NASA Technical Memorandum.

25. Dayton, B.B., "Gas Flow Patterns at Entrance and Exit of Cylindrical Tubes," *National Symposium on Vacuum Technology Transactions*, Pergamon Press, New York, NY, 1956, pp 5–11.
26. Williams, G.J., Smith, T.B., Domonkos, M.T., Shand, K.J., Gallimore, A.D., and Drake, R.P., "Laser Induced Fluorescence Characterization of Ions Emitted from Hollow Cathode," AIAA 99–2862, 35th Joint Propulsion Conference, Los Angeles, CA, Jun. 20–23, 1999.
27. Mikellides, I.G., Katz, I., Goebel, D.M., and Polk, J.E., "Hollow Cathode Theory and Experiment II: A Two-Dimensional Theoretical Model of the Emitter Region," Journal of Applied Physics 98, 113303, 2005.
28. Mikellides, I.G., Katz, I., Goebel, D.M., and Polk, J.E., "Theoretical Model of a Hollow Cathode Insert Plasma," AIAA–2004–3817, 40th Joint Propulsion Conference, Ft Lauderdale, FL, Jul. 11–14, 2004.
29. Polk, J.E., Goebel, D.M., Snyder, J.S., Schneider, A.C., Johnson, L.K., and Sengupta, A., "Performance and Wear Test Results for a 20 kW-Class Ion Engine with Carbon-Carbon Grids," AIAA–2005–4393, 41st Joint Propulsion Conference, Tucson, AZ, Jul. 10–13, 2005.
30. Van Noord, J.L., "NEXT Ion Thruster Thermal Model," AIAA–2007–5218, 41st Joint Propulsion Conference, Tucson, AZ, Jul. 10–13, 2005.
31. Williams, G.J., "The Use of Laser-Induced Fluorescence to Characterize Discharge Cathode Erosion in a 30 cm Ring-Cusp Ion Thruster," NASA/CR—2004-211296, Apr. 2004, p. 116.
32. Boyd, I.D. and Dressler, R.A., "Far Field Modeling of the Plasma Plume of a Hall Thruster," Journal of Applied Physics, Vol. 92, No. 4, Aug. 15, 2002, pp. 1764–1774.
33. Miller, J.S., Pullins, S.H., Levandier, D.J., Chiu, Y., and Dressler, R.A., "Xenon Charge Exchange Cross Sections for Electrostatic Thruster Models," Journal of Applied Physics, Vol. 91, No. 3, Feb. 1, 2002, pp. 984–991.
34. Herman, D.A. and Gallimore, A.D., "Discharge Chamber Plasma Structure of a 30-cm NSTAR-type Ion Engine," AIAA–2004–3794, 40th Joint Propulsion Conference, Ft. Lauderdale, FL, Jul. 11–14, 2004.
35. Aston, G. and Wilbur, P.J., "Ion Extraction from a Plasma," Journal of Applied Physics, 52(4), Apr. 1981, pp. 2614–2626.
36. Farnell, C.C., Williams, J.D., and Wilbur, P.J., "Characteristics of Energetic Ions Emitted from Hollow Cathodes," IEPC 03–072, 28th International Electric Propulsion Conference, Toulouse, France, Mar. 17–21, 2003.
37. Jameson, K.K., Goebel, D.M., and Watkins, R.M., "Hollow Cathode and Keeper-Region Plasma Measurements," AIAA–2005–3667, 41st Joint Propulsion Conference, Tucson, AZ, Jul. 10–13, 2005.
38. Foster, J.E. and Patterson, M.J., "Characterization of Downstream Ion Energy Distributions from a High Current Hollow Cathode in a Ring Cusp Discharge Chamber," AIAA–2003–4865, 39th Joint Propulsion Conference, Huntsville, AL, Jul. 20–23, 2003.
39. Bevington, P.R., *Data Reduction and Error Analysis for the Physical Sciences*, McGraw-Hill, New York, NY, 1969, Ch. 4.

REPORT DOCUMENTATION PAGE	Form Approved OMB No. 0704-0188

1. REPORT DATE *(DD-MM-YYYY)*	2. REPORT TYPE	3. DATES COVERED *(From - To)*
01-11-2010	Technical Memorandum	

4. TITLE AND SUBTITLE
Thrust Stand Characterization of the NASA Evolutionary Xenon Thruster (NEXT)

5a. CONTRACT NUMBER

5b. GRANT NUMBER

5c. PROGRAM ELEMENT NUMBER

6. AUTHOR(S)
Diamant, Kevin, D.; Pollard, James, E.; Crofton, Mark, W.; Patterson, Michael, J.; Soulas, George, C.

5d. PROJECT NUMBER

5e. TASK NUMBER

5f. WORK UNIT NUMBER
WBS 346620.04.08.02.02.01

7. PERFORMING ORGANIZATION NAME(S) AND ADDRESS(ES)
National Aeronautics and Space Administration
John H. Glenn Research Center at Lewis Field
Cleveland, Ohio 44135-3191

8. PERFORMING ORGANIZATION REPORT NUMBER
E-17474

9. SPONSORING/MONITORING AGENCY NAME(S) AND ADDRESS(ES)
National Aeronautics and Space Administration
Washington, DC 20546-0001

10. SPONSORING/MONITOR'S ACRONYM(S)
NASA

11. SPONSORING/MONITORING REPORT NUMBER
NASA/TM-2010-216895

12. DISTRIBUTION/AVAILABILITY STATEMENT
Unclassified-Unlimited
Subject Category: 20
Available electronically at http://gltrs.grc.nasa.gov
This publication is available from the NASA Center for AeroSpace Information, 443-757-5802

13. SUPPLEMENTARY NOTES

14. ABSTRACT
Direct thrust measurements have been made on the NASA Evolutionary Xenon Thruster (NEXT) ion engine using a standard pendulum style thrust stand constructed specifically for this application. Values have been obtained for the full 40-level throttle table, as well as for a few off-nominal operating conditions. Measurements differ from the nominal NASA throttle table 10 (TT10) values by 3.1 percent at most, while at 30 throttle levels (TLs) the difference is less than 2.0 percent. When measurements are compared to TT10 values that have been corrected using ion beam current density and charge state data obtained at The Aerospace Corporation, they differ by 1.2 percent at most, and by 1.0 percent or less at 37 TLs. Thrust correction factors calculated from direct thrust measurements and from The Aerospace Corporation's plume data agree to within measurement error for all but one TL. Thrust due to cold flow and "discharge only" operation has been measured, and analytical expressions are presented which accurately predict thrust based on thermal thrust generation mechanisms.

15. SUBJECT TERMS
Ion thruster; Ion engine

16. SECURITY CLASSIFICATION OF:			17. LIMITATION OF ABSTRACT	18. NUMBER OF PAGES	19a. NAME OF RESPONSIBLE PERSON
a. REPORT	b. ABSTRACT	c. THIS PAGE			STI Help Desk (email:help@sti.nasa.gov)
U	U	U	UU	25	19b. TELEPHONE NUMBER *(include area code)* 443-757-5802